Polymer 149 (2018) 13–22

Contents lists available at ScienceDirect

Polymer

journal homepage: www.elsevier.com/locate/polymer

3-D magnetic graphene oxide-magnetite poly(vinyl alcohol) nanocomposite substrates for immobilizing enzyme

Yanyun Li [a], Tao Jing [a, *], Gaofeng Xu [b, **], Jingzhi Tian [a], Mengyao Dong [c], Qian Shao [d], Bin Wang [e], Zhikang Wang [f, ***], Yongjie Zheng [a], Changlong Yang [a], Zhanhu Guo [c, ****]

[a] College of Chemistry and Chemical Engineering, Qiqihar University, Qiqihar, 161006, China
[b] College of Chemical Engineering, Southwest Forestry University, Kunming, Yunnan, 650224, China
[c] Integrated Composites Laboratory (ICL), Department of Chemical & Biomolecular Engineering, University of Tennessee, Knoxville, TN, 37934, USA
[d] Engineered Multifunctional Composites (EMC) Nanotech. LLC, Knoxville, TN, 37934, USA
[e] College of Chemical and Environmental Engineering, Shandong University of Science and Technology, Qingdao, Shandong, 266590, China
[f] College of Eco-environmental Engineering, Guizhou Minzu University, Guiyang, Guizhou, 550025, China

ARTICLE INFO

Article history:
Received 8 May 2018
Received in revised form
4 June 2018
Accepted 16 June 2018
Available online 18 June 2018

Keywords:
3D-graphene oxide
Magnetic
Enzyme
Adsorption
Stability of enzyme activity

ABSTRACT

Three-dimensional magnetic graphene oxide-magnetite polyvinyl alcohol (3D-GO/PVA/Fe_3O_4) nanocomposites were successfully prepared. The morphology was characterized and analyzed through scanning electron microscope (SEM) and transmission electron microscope (TEM). The chemical structure and the crystal structure were explored by X-ray powder diffraction (XPS), Fourier transform infrared spectroscopy (FT-IR) and X-ray diffraction spectra (XRD). The magnetic property was obtained by vibrating sample magnetometer (VSM). The specific surface area and the average pore size were determined by Brunauer-Emmett-Teller (BET) and Barrett–Joyner–Halenda (BJH). The specific surface and the average pore size of 3D-GO/PVA/Fe_3O_4 nanocomposites were 388.87 m^2g^{-1} and 9.6 nm, and the higher specific surface indicated that the three-dimensional structure avoided the aggregation for GO sheets. The large saturation magnetization (M_s) of the nanocomposites of 30.5 emu/g enabled the easy cycling of the nanocomposites. The 3D-GO/PVA/Fe_3O_4 nanocomposites exhibited better performance for porcine pancreatic lipase (PPL) enzyme immobilization. The maximum immobilization efficiency was 91%, and the enzyme immobilized 3D-GO/PVA/Fe_3O_4 nanocomposites reached up to 90% of their activities. After 10 cycles of reuse, the activity of immobilized enzyme remained about 70.8% of the initial activity. The stability test revealed that the activity of immobilized enzyme remained up to 71.1% at 4 °C for 56 days.

1. Introduction

Free enzymes have the disadvantages of easy deactivation, low stability, difficulty in separation from the product, and low reusability during the catalytic reaction, thus limit the further applications of lipase. Enzyme immobilization technology can solve these problems. It enables the reusage of enzymes and reduces the costs. The unique characteristics of the immobilized materials are designed to make enzymes fully exhibit catalytic activity, improve the stability of enzymes at high temperature and under acid and alkali environments, increase the reuse rate of enzymes, and reduce the production cost. Two-dimensional graphene oxide (2D-GO) is a kind of nanomaterials with a large number of oxygen-containing functional groups such as hydroxyl, carboxyl and epoxy groups [1–4], and thus can be well dispersed in water. These oxygen-containing groups in 2D-GO make it possible to immobilize enzymes without modifying the GO without using any surfactant or coupling agent. 2D-GO has a large specific surface area, good mechanical properties, and high biocompatibility [5–8]. These unique properties make GO ideal substrates for studying the enzyme immobilization. However, 2D-GO is prone to agglomerate by van der Waals, so that a large number of active sites are lost [9,10], and thus affects its performance as a matrix. Some stabilizers [11] are

* Corresponding author.
** Corresponding author.
*** Corresponding author.
**** Corresponding author.
E-mail addresses: jtkr@163.com (T. Jing), xgf0208@163.com (G. Xu), wzk_gzmz@163.com (Z. Wang), zguo10@utk.edu (Z. Guo).

https://doi.org/10.1016/j.polymer.2018.06.046
0032-3861/

often added into GO to prevent the agglomeration [12], however, the specific surface area of GO will be reduced, which will influence the performance of 2D-GO.

In order to overcome the disadvantages of 2D-GO, various of 3D-GO composites had been prepared for a wide range of applications including the lithium ion batteries [13,14], supercapacitors [15,16], solar cells and fuel cells [17–19], co-catalysis [20,21], thermal interface material [22–24], sensors [25–30], enrichment and separation [31,32], and others [33–37].

Polymers, which are polyethylene-allylamine (PEI) [38], polyvinyl alcohol (PVA) [39], polyvinylidene fluoride (PVDF) [40], poly (m-phenylenediamine) (PmPD) [41] and poly (acrylic acid) (PAA) [42] have been shown to significantly assist GO self-assembly into 3D graphene macrostructures with excellent properties. Electrostatic interactions and hydrogen bonding are suggested as forces between the oxygen-containing groups on the GO and the functional groups on the polymers (-NH_2 or -OH) [43,44]. The assembly of graphene into a 3D hierarchy is considered one of the most promising strategies for “bottom-up" nanotechnology [45]. PVA is a hydroxyl-rich material, and provides more binding sites for the enzyme immobilization [46] to improve immobilization efficiency of the enzyme. Doğaç et al. [47] successfully immobilized lipase on PVA/alginate and polyethylene oxide/alginate nanofibers. Results showed that nanofibers (especially PVA/alginate) enhanced the stability properties of lipase. When the free lipase lost its all activity after 40–60 min at high temperatures, both lipase immobilized nanofibers kept almost 65–70% activity at the same time. The polymer has a large specific surface area as an immobilized carrier. However, the spatial structure did not consider whether the conformation of the enzyme would have an impact. In addition, it should be emphasized that Fe_3O_4 nanoparticles (Fe_3O_4 NPs) were also used to make the novel composites, which will made the novel composites obtain good magnetic property and could be easily isolated from reaction medium by using a magnet [48]. Shao et al. [49] prepared GO/Fe_3O_4 composites. Under the optimal conditions pH 7.5, enzyme concentration of 0.25 mg/mL and the temperature of 25 °C, the best immobilized efficiency was 76%, and at 60 °C the enzyme activity kept 69%. But due to the limitation of specific surface area of the composite material, the immobilization efficiency and activity of the enzyme are affected.

In this paper, 3D-GO/PVA/Fe_3O_4 composites were prepared and were used for immobilizing enzyme. The immobilization efficiency of enzyme and enzyme activity were analyzed based on varied conditions, such as temperature, enzyme concentration, pH and adsorption time. The reusability and storage stability of immobilized enzyme were also investigated.

2. Experimental

2.1. Materials

Griphene (325 mesh) was purchased form Jinrilai graphite Inc, (Qingdao, China). Olive oil was obtained from Aladdin (Shanghai, China). Potassium permanganate ($KMnO_4$), iron (III) chloride hexahydrate ($FeCl_3 \cdot 6H_2O$), ethylene glycol, sodium acetate, absolute ethanol, absolute toluene, and polyvinyl alcohol (PVA) were obtained from Kemi Ou Chemical Reagent Co., (Tianjin, China). Porcine pancreas lipase (PPL) (EC3.1.1.3) enzyme was purchased from Sinopharm Chemical Reagent Co., Ltd (Shanghai, China). Phosphate buffer saline (PBS) was prepared by the solutions of NaH_2PO_4 and Na_2HPO_4. All the chemicals were of analytical grade.

2.2. Preparation of graphene oxide (GO)

Two-dimensional graphene oxide (2D-GO) was prepared with modified Hummers method [50–52]. Briefly, 3 g sodium nitrate, 5 g graphite, and 120 mL concentrated sulfuric acid were gradually added to a three-necked flask in an ice-water bath. Then, 20 g $KMnO_4$ were slowly added into the three-necked flask over 1 h, and the mixture was stirred for another 2 h. The mixture was maintained in a warm water bath (35 °C) for 0.5 h, and 230 mL deionized water was dropwise added into the mixture in an ice-water bath. The flask was transferred to a water bath (98 °C) for 20 min and then transferred to room temperature. H_2O_2 was added to remove excess $KMnO_4$ from the mixture, and washed with dilute hydrochloric acid, and the supernatant was verified with $BaCl_2$ solution only with no precipitation, and then washed with deionized water to neutral. The obtained sample was dried in vacuum at 60 °C to obtain graphene oxide.

2.3. Preparation of Fe_3O_4 nanoparticles

In this study, Fe_3O_4 nanoparticles (Fe_3O_4 NPs) were prepared by solvothermal method as followed [53]. Firstly, 2.2 g $FeCl_3 \cdot 6H_2O$ and 80 mL ethylene glycol were mixed by stirring until completely dissolved. Then, a mixture of NaAc/sodium citrate (25:1) was added to the above solution. The solution was transferred to a stainless-steel autoclave and kept 200 °C for 20 h Fe_3O_4 NPs were washed with anhydrous ethanol and dried in vacuum.

2.4. Preparations of 3D-GO/PVA and 3D-GO/PVA/Fe_3O_4 composites

Preparation of 3D-GO/PVA composites: The GO dispersion with a concentration of 6 mg/mL was prepared, and then PVA (0.012 g) was added in the solution with ultra-sonication for 1 h, which was named as GO/PVA hydrogels, afterwards, toluene (10 mL) were added to the solution with ultra-sonication for 1 h. After freeze-dried, the mixtures were collected and stored, which was named as 3D-GO/PVA composites.

Preparation of 3D-GO/PVA/Fe_3O_4 composites: Fe_3O_4 NPs (0.08 g) were immersed into 10 mL toluene with ultra-sonication. Then, the 10 mL mixture (Fe_3O_4/toluene) was added into GO/PVA hydrogels (prepared above). The mixtures of GO/PVA/Fe_3O_4/toluene were continuously ultra-sonication for 2 h. Finally, the preparation of 3D-GO/PVA/Fe_3O_4 composites was finished by freeze drying.

2.5. Immobilization of PPL on 3D-GO/PVA/Fe_3O_4 composites

3D-GO/PVA/Fe_3O_4 composites (0.14 g) were added into the PBS buffer (10 mL, 0.05 M, pH 7.5) and ultra-sonicated for 1 h. The solution of PPL (3.5 mg/mL, 10 mL) and 3D-GO/PVA/Fe_3O_4 were mixed and shaken at 120 rpm for 6 h at 30 °C. Then, the mixture of (3D-GO/PVA/Fe_3O_4)-PPL was washed by PBS buffer and collected using magnet.

2.6. Determination of immobilization efficiency for (3D-GO/PVA/Fe_3O_4)-PPL

The immobilization efficiency for (3D-GO/PVA/Fe_3O_4)-PPL was determined through Bradford method [49,54], and the immobilization efficiency would be obtained by the BSA standard curve. To obtain the best immobilization efficiency, the immobilization conditions were optimized, such as the time of immobilization (2–16 h), concentration of PPL (2–5.5 mg/mL) and reaction temperature (25–60 °C).

The immobilization efficiency is calculated by Formula (1):

$$\text{Immobilization efficiency } (\%) = \frac{\text{total of content (mg)-PPL in supernatant (mg)}}{\text{total of content (mg)}} \times 100\% \quad (1)$$

2.7. Activity assay

The activity assay on the immobilized enzyme was investigated by olive oil emulsification method [55]. Briefly, PVA emulsion (0.03 g/mL) was prepared first. Then the PVA-olive oil emulsion (20%) was prepared by mixing PVA emulsion with olive oil. PVA-olive oil emulsion (5 mL), 3 mL PBS buffer and 15 mL 95% ethanol were mixed in a flask, which was named as blank flask (A). Additionally, a sample flask (B) was prepared as described above but without adding ethanol. The flasks of A and B were heated at 40 °C for 5 min and the enzyme solution (1 mL) was added for 15 min. Afterwards, 95% ethanol (15 mL) was added into flask (B) to terminate the reaction. Finally, the solutions from (A and B) were titrated with 0.05 M NaOH.

One unit (U) of enzyme activity is defined as the amount of lipase consumed to produce 1 μmol fatty acid per minute. The used formula (2) is as follows:

$$U = \frac{V\text{-}V_0}{t \times M \times n} \quad (2)$$

where V_0 and V represent the consumption of NaOH solution at the flask of A and B, and t represents reaction time. M is the number of micrograms that contained in 1 mL NaOH standard solution. n is multiple of dilution.

2.8. Effects of the temperature, enzyme concentration and pH on the relative activity

To study the effects of the temperature, enzyme concentration and pH for free and immobilized enzymes, various conditions were applied for enzyme activity testing, including the temperature ranging from 25 to 60 °C, enzyme concentration ranging from 2 to 5.5 mg/mL, and pH ranging from 5.5 to 9.0, respectively. Enzyme activity assay was done using the same report method [55].

2.9. Reusability and storage stability of immobilized enzyme

To probe the reusability of immobilized enzyme, the immobilized enzyme was reused 6 times to compare the enzyme activity after each use.

To evaluate the storage stability of immobilized enzyme, the free and immobilized enzymes were stored in a refrigerator at 4 °C. The enzyme activities were measured every seven days for 8 times (total 56 days) and compared the testing results.

2.10. Methods for characterizations

The surface morphologies of the composites were characterized by scanning electron (SEM) microscope (Hitachi S-4300, Japan), and transmission electron (TEM) microscopy (Hitachi S-7650, Japan). The crystal and chemical structures for composites were analyzed by X-ray photoelectron spectroscopy (XPS) (Thermo Fisher, USA) and X-ray diffraction (XRD, Bruker D8-FOCUS, Germany) spectra. XRD spectra were obtained with Cu $K\alpha$ radiation and the 2θ angle range of 10–80° with the step-width 0.02°. The groups for composites were detected by Fourier transform infrared (FT-IR) spectroscopy using for KBr tabletting at the range of 500–4000 cm^{-1} (PE Spectrum One B, USA). Magnetic property for magnetic material was determined by vibrating sample magnetometer (VSM) at room temperature and test range from −30000 to 30000 Oe (VersaLab VL-072, USA). Nitrogen adsorption/desorption (AUTOSORB-1, USA) was applied to determine the pore size and the surface area for composites. The composites before testing should be degassed under vacuum for 3 h. Thermogravimetric analysis (TGA) (NETZSCH STA 449 F3, Germany) was conducted to measure the thermal stability of composites in nitrogen atmosphere with increasing from 0° to 800° at a ramp rate of 10 °C/min. All of the composites prepared were dried by freeze-drying (Shengchao LGJ-10, China) (Fig. 1)

3. Results and discussion

3.1. Characterization on the materials

3.1.1. Morphology of GO, Fe_3O_4 NPs, 3D-GO/PVA and 3D-GO/PVA/Fe_3O_4 composites

The morphologies of GO, Fe_3O_4 NPs, 3D-GO/PVA and 3D-GO/PVA/Fe_3O_4 composites were explored by SEM and TEM. Fig. 2a shows a typical SEM structure for GO, with thin lamellar, edge curl and more wrinkles. The TEM image also displays the thin and transparent layers of GO (Fig. 2b), which was consistent with the other reports [56–58]. Both SEM and TEM images show that Fe_3O_4 NPs were lychee-like spherical structure and evenly dispersed and uniform particles (Fig. 2c and d).

The morphology of 3D-GO/PVA composites is shown in Fig. 2 (e and f), and the morphology of 3D-GO/PVA/Fe_3O_4 composites is shown in Fig. 2 (g and i). PVA in the composites acted as a cross-linking agent, and PVA chains could conjugate with one or more GO nanosheets to form 3D-GO/PVA (Fig. 2e and f), presenting a three-dimensional and porous structure. The structure was composed of PVA and thin-layer GO, which reduced the agglomeration of GO and provided more active sites. The images for 3D-GO/PVA/Fe_3O_4 composites (Fig. 2g–i) clearly depict that Fe_3O_4 NPs were loaded onto GO nanosheets successfully, so that the magnetic property was endowed to the composites. This can be used to collect the composites and prevent further aggregates of GO [12,59,60].

3.1.2. Magnetization property testing for Fe_3O_4 NPs and the 3D-GO/PVA/Fe_3O_4 composites

The magnetization property of Fe_3O_4 NPs or 3D-GO/PVA/Fe_3O_4 composites was tested using VSM at room temperature. The magnetization curves of 3D-GO/PVA/Fe_3O_4 composites are shown in Fig. 3. The hysteresis loop shows a typical S-shape and the coercivity is about 7.2 Oe for Fe_3O_4 NPs. A very small but nonzero value indicates that the Fe_3O_4 NPs exhibit quasi-superparamagnetic properties with small coercivities (Fig. 3a) [61]. In the picture, the saturation magnetization (M_s) of the 3D-GO/PVA/Fe_3O_4 composites (Fig. 3b) is 30.5 emu/g, which is lower than that of pure Fe_3O_4 NPs (110.5 emu/g) (Fig. 3b). According to the literature reported by other researchers [62], the M_s of Fe_3O_4 could be reduced due to the presence of GO. Therefore, the phenomenon proved further that Fe_3O_4 NPs were successfully loaded on the surface of GO [58] and made the composites magnetic, and the composites could be

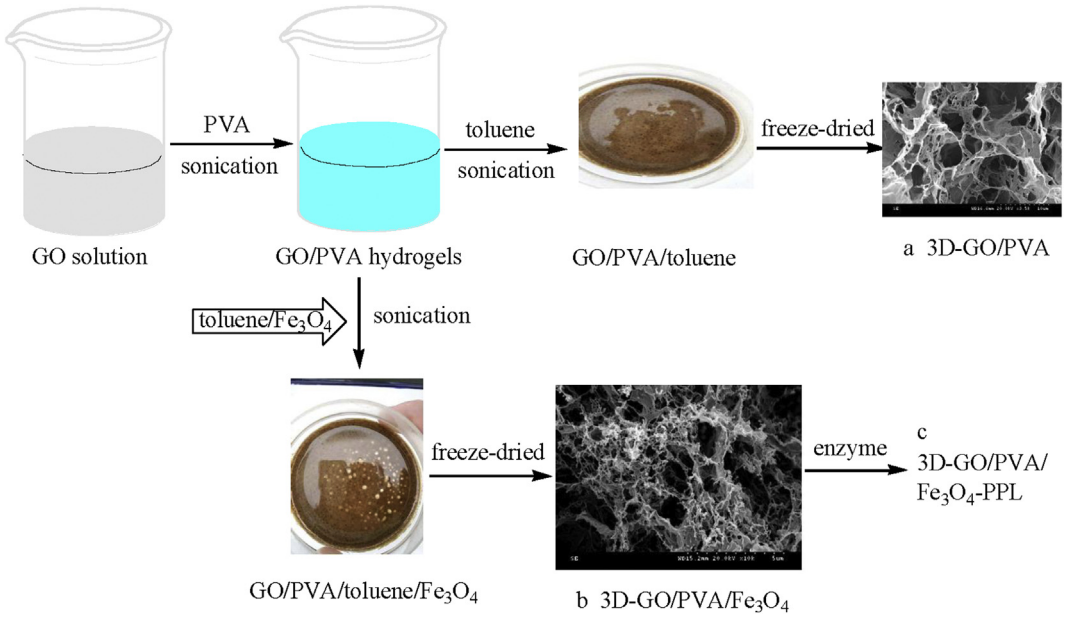

Fig. 1. Schematic representation of the formation of (a) 3D-GO/PVA, (b) 3D-GO/PVA/Fe_3O_4 and (c) 3D-GO/PVA/Fe_3O_4-PPL.

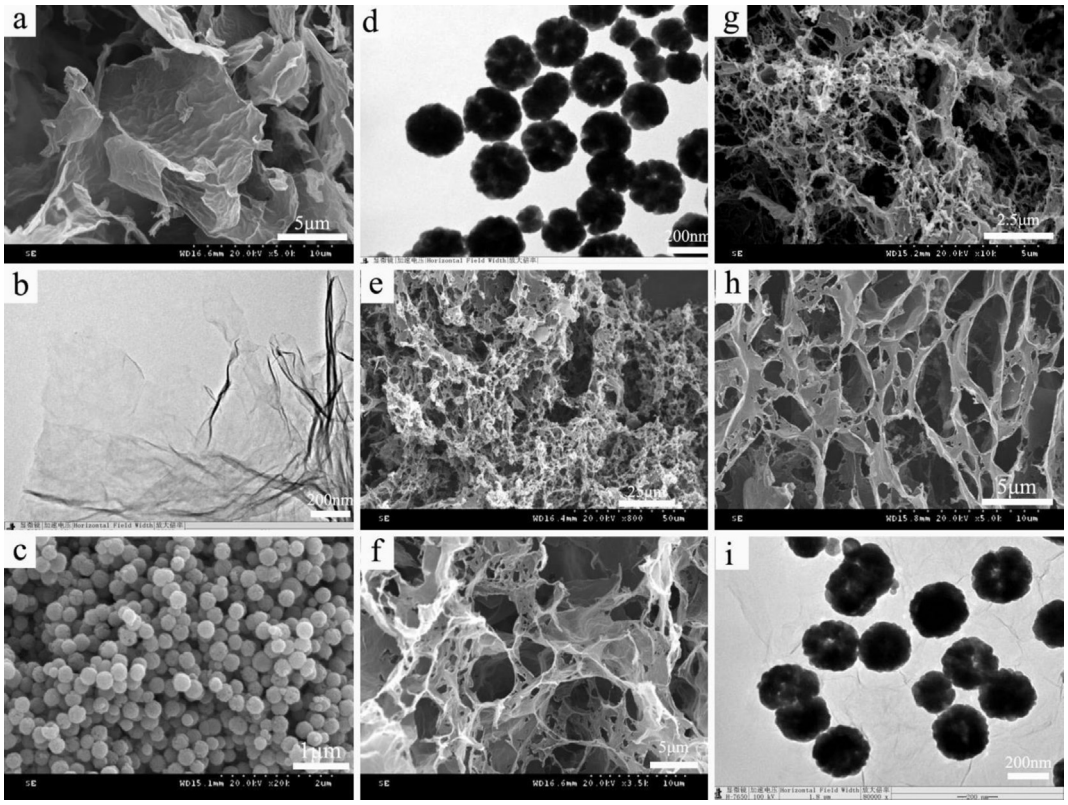

Fig. 2. SEM microstructure of GO (a). TEM image of GO (b). SEM images of Fe_3O_4NPs (c and d, average particle size was about 270 nm). SEM images of 3D-GO/PVA (e and f), SEM images of 3D-GO/PVA/Fe_3O_4 composites (g and h), TEM microstructure of 3D-GO/PVA/Fe_3O_4 composites (i).

enough separated from the solution with a magnet [63].

3.1.3. *The specific surface area and pore size distribution of the 3D-GO/PVA/Fe_3O_4 composites*

The specific surface area and pore size of the 3D-GO/PVA/Fe_3O_4 composites were investigated using BET and BJH method by the nitrogen adsorption/desorption isotherm analysis. The isotherm of the 3D-GO/PVA/Fe_3O_4 composites exhibited a hysteresis loop similar to type IV, and indicated that the capillary condensation phenomenon of the mesoporous structure on the composites appeared. BET analysis showed a specific surface area for the 3D-GO/PVA/Fe_3O_4 composites of 388.87 $m^2 g^{-1}$ (Fig. 4),

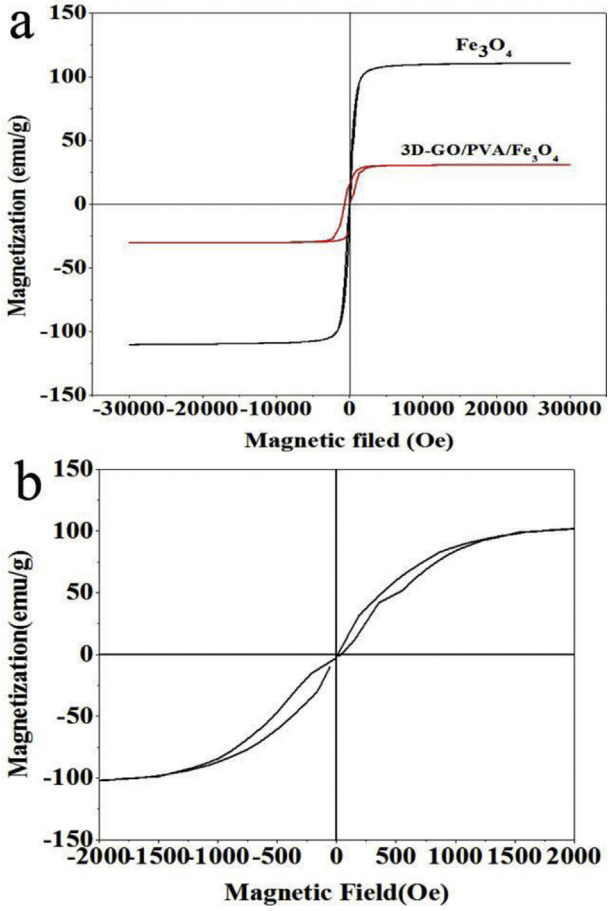

Fig. 3. Magnetization curves of Fe_3O_4 NPs and 3D-GO/PVA/Fe_3O_4 composites (a). Enlarged magnetization curve of Fe_3O_4 NPs (b).

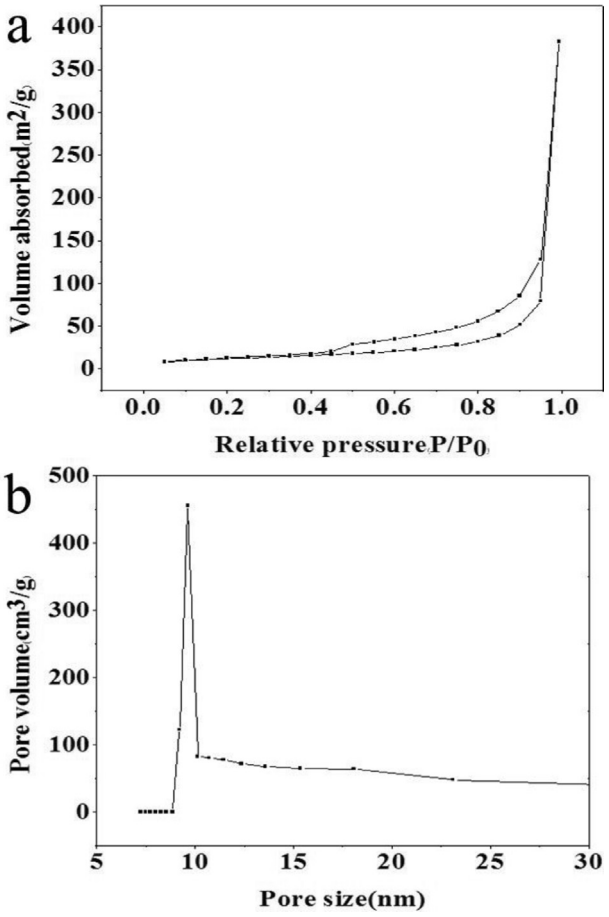

Fig. 4. The specific surface area and pore size of the 3D-GO/PVA/Fe_3O_4 composites.

which was higher than that of 2D-GO/Fe_3O_4 [12]. The higher specific surface area of 3D-GO/PVA/Fe_3O_4 composites were attributed to the particular three dimensional network structure, which avoided the problems of the aggregation or restacking by strong van der Waals interactions between GO sheets. The pore size of the 3D-GO/PVA/Fe_3O_4 composites was analyzed by BJH method, and the average pore size of the sample was approximately 9.6 nm (Fig. 4).

3.1.4. XPS analysis for 3D-GO/PVA/Fe_3O_4 composites

The chemical structure of the composites was analyzed by XPS. As shown in Fig. 5a, two peaks of C 1s and O 1s appeared for GO, implying that GO contained two elements of C and O. In the C 1s spectrum (Fig. 5d), three curve-fitted peaks were distinguished, and they were C-C/C=C at 284.8 eV, C=O at 288.7 eV, and C-O at 286.8 eV, meaning that GO was prepared successfully [64]. After adding PVA, it was noticed that the intensity of C-C/C=C in 3D-GO/PVA composites (Fig. 5e) was increased than that of GO, suggesting that PVA reacted with GO. Meanwhile, the C=O and C-O binding energies of 3D-GO/PVA compared with that of GO decreased by 0.12 eV and 0.12 eV (Fig. 5e), indicating the involvement of electron donors. This was due to that C=O and C-O in GO and -OH in PVA formed hydrogen bond, and the electron cloud shifted to O atoms on C=O and C-O functional groups, resulting in an increase in the electron density of O atoms and thus a reduced binding energy. XPS spectra of 3D-GO/PVA/Fe_3O_4 composites show that the element of Fe appeared except C and O, this indicated the loading of Fe_3O_4 on the composites [60]. The spectra of Fe_3O_4 NPs (Fig. 5g) from composites show two peaks corresponding to the spin orbit peaks for Fe $2p_{3/2}$ and Fe $2p_{1/2}$ from pure Fe_3O_4 [12], which were located at 711.2 and 724.8 eV, rather than at 710.3 and 724.0 eV (γ-Fe_2O_3) [65]. Moreover, it demonstrated that Fe_3O_4 was conjugated into the composites [64]. Meanwhile, the intensity of C-O in the C 1s spectrum of 3D-GO/PVA/Fe_3O_4 composites (Fig. 5f) was found to be lowered compared to the 3D-GO/PVA composites, further suggesting that Fe_3O_4 NPs were successfully anchored on the surface of GO nanosheets [66].

3.1.5. XRD analysis

The crystal structures of GO, 3D-GO/PVA composites, and 3D-GO/PVA/Fe_3O_4 composites were also explored in Fig. 6. The XRD pattern of GO (Fig. 6A) exhibits an obvious diffraction peak at $2\theta = 11.94°$, which corresponds to the crystal planes of (001) [67]. Graphite diffraction peaks (002) that were not oxidized at $2\theta = 26°$ were not found, indicating that the GO prepared in this experiment was oxidized completely. It indicated that many oxygen-containing functional groups existed on the surface of GO. According to the Bragg equation and $2\theta = 11.94°$, the interlayer spacing of GO was calculated, and it was 0.74 nm. As shown in Fig. 6B, the diffraction peak of 3D-GO/PVA composites was $2\theta = 15.46°$, and the interlayer spacing was 0.57 nm. This indicated that PVA inserted into the GO layer space [68], leading to the change on the interlayer spacing. Furthermore, the characteristic diffraction peak of PVA (101) at 3D-GO/PVA and 3D-GO/PVA/Fe_3O_4 composites showed weaker diffraction peak intensity at $2\theta = 19–20°$, because of the lower

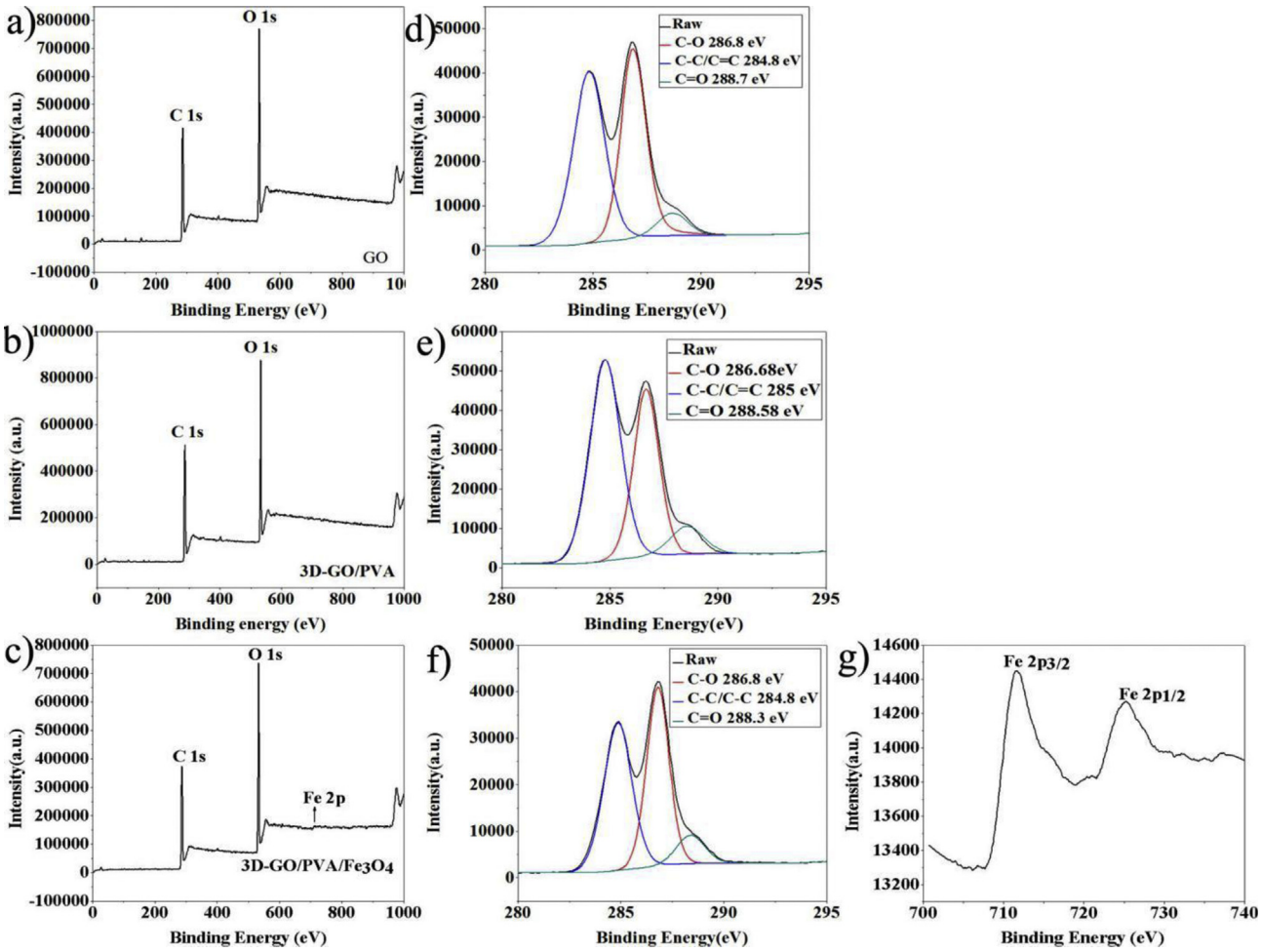

Fig. 5. XPS spectra of GO (a), 3D-GO/PVA (b) and 3D-GO/PVA/Fe_3O_4 (c). The high-resolution C1s spectrum of GO (d), 3D-GO/PVA (e) and 3D-GO/PVA/Fe_3O_4 (f), respectively. The high-resolution Fe 2p spectrum of Fe_3O_4 from the composites (g).

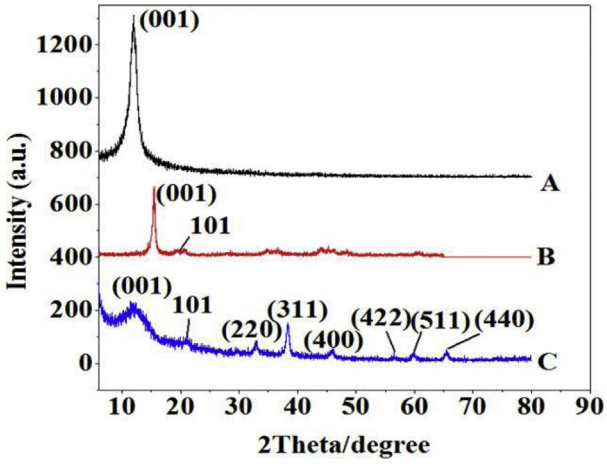

Fig. 6. XRD patterns of GO (A), 3D-GO/PVA composites (B), and 3D-GO/PVA/Fe_3O_4 composites (C).

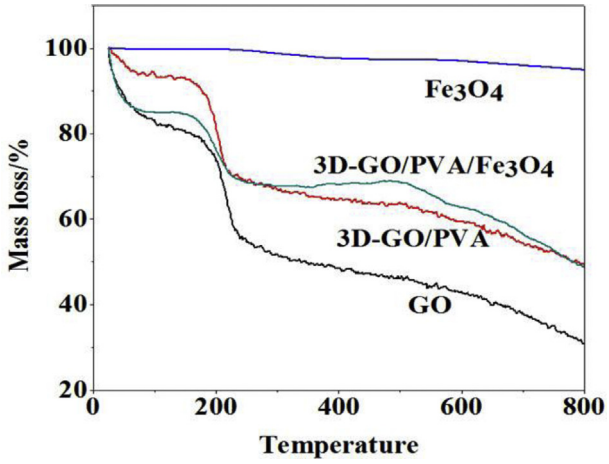

Fig. 7. TGA curves of Fe_3O_4, GO, 3D-GO/PVA, 3D-GO/PVA/Fe_3O_4 composites.

amount of PVA. As shown in Fig. 6c, 3D-GO/PVA/Fe_3O_4 composites had seven diffraction peaks, except the diffraction peak for GO (001), all of other six weaker peaks were the characteristic peaks of Fe_3O_4, i.e., 30.1°, 35.4°, 43.0°, 53.5°, 57.0°, and 62.5°, respectively. The crystal planes corresponded to 220, 311, 400, 422, 511, and 440, which were consistent with the face-centered cubic (fcc) structure of Fe_3O_4 [63], indicating that Fe_3O_4 was loaded on the GO surface. The (001) peak becomes broad and weak in the 3D-GO/PVA/Fe_3O_4 nanocomposites. It may be due to the formation of 3D-GO/PVA/Fe_3O_4 that leads to poor ordering during the stacking of GO sheet [69].

3.1.6. TGA properties of Fe_3O_4 NPs, GO, 3D-GO/PVA, 3D-GO/PVA/Fe_3O_4 composites

The thermal stability of Fe_3O_4 NPs, GO, 3D-GO/PVA, 3D-GO/PVA/Fe_3O_4 composites were detected by TGA. As shown in Fig. 7, Fe_3O_4 NPs showed good thermal stability within the temperature range from 0 to 800 °C. TGA curves of the GO, 3D-GO/PVA and 3D-GO/PVA/Fe_3O_4 composites exhibited three stages on the weight loss. For GO, the first stage at 0–190 °C of the weight loss was ascribed to the loss of adsorbed water [70,71]. The TGA curve (Fig. 7) shows a downward trend at the second stage in the range of 150–250 °C. This may be due to the thermal decomposition of oxygen-containing groups in GO to CO_2, CO and H_2O [72,73]. In addition, the TGA curve shows a downward trend at the third stage (250–650 °C) due to the thermal decomposition of the remaining GO after removing the oxygen-containing groups [74].

The first stage for 3D-GO/PVA composites at 0–190 °C was lost due to the physically adsorbed water in Fig. 7. The second stage of 3D-GO/PVA composites was at 190–220 °C. Compared to pure GO, the degradation temperature of 3D-GO/PVA composites decreased. The weight loss of 3D-GO/PVA composites below 220 °C was mainly the decomposition of oxygen-containing functional groups on PVA and GO. The third stages at 220–630 °C was mainly PVA backbone decomposition and GO carbon skeleton pyrolysis. For the 3D-GO/PVA/Fe_3O_4 composites, the second stage was the same as 3D-GO/PVA composites. The temperature of the third stage moved to the right, and it showed that the addition of Fe_3O_4 improved the thermal stability of 3D-GO/PVA.

3.1.7. FT-IR. Spectra analysis on PVA, GO, 3D-GO/PVA, Fe_3O_4 NPs, 3D-GO/PVA/Fe_3O_4, PPL and (3D-GO/PVA/Fe_3O_4)-PPL composites

The functional group analysis of several samples was explored by the FT-IR spectra as shown in Fig. 8. The characteristic peaks of GO (Fig. 8A_2) were located at ~1719, ~1624, ~1398, and ~1063 cm^{-1}, which corresponded to the stretching vibrations of C=O, C=C, C-OH, and C-O, respectively [75–78]. The broad band at ~3481 cm^{-1} was related to the vibration bands of -OH [79] (Fig. 7A). The peak at ~2942 cm^{-1} was attributed to the C-H stretching vibration of methylene groups in PVA (Fig. 8A_5), which also appeared in the 3D-GO/PVA and 3D-GO/PVA/Fe_3O_4 composites (Fig. 8A_3 and 8A_4). The peak intensity of the C=O functional group on 3D-GO/PVA was significantly reduced compared to GO, which was due to the formation of hydrogen bonds between -OH of PVA and C=O of GO. The characteristic peak at 584 cm^{-1} was attributed to the Fe-O bending vibration from Fe_3O_4 NPs [48] (Fig. 8A_1), which also appeared in the 3D-GO/PVA/Fe_3O_4 (Fig. 8A_4), indicating that Fe_3O_4 NPs were anchored on GO nanosheets successfully.

As shown in Fig. 7B_7, the bands at 1643, and 1543 cm^{-1} were assigned to the -CO-NH- group in PPL [80,81]. Meanwhile, the immobilized enzyme also had an amino absorption peak at the same position (Fig. 8B_6), demonstrating that PPL was successfully immobilized on the 3D-GO/PVA/Fe_3O_4 composites [82,83]. Additionally, the transmittance for the O-H band (3389 cm^{-1}, Fig. 8B) of enzyme inn the composites was weakened, indicating that an interaction by hydrogen bonding occurred between PPL and 3D-GO/PVA/Fe_3O_4 composites [12].

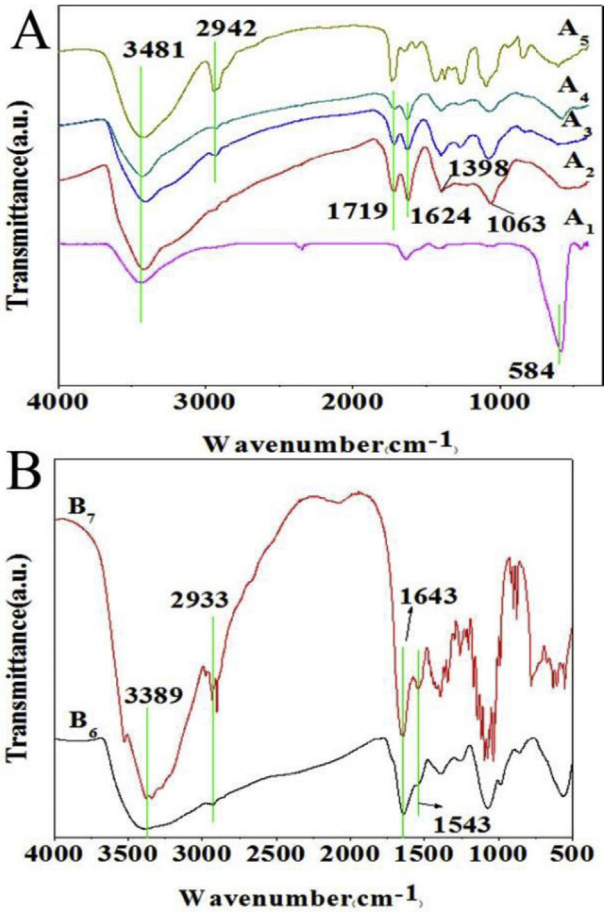

Fig. 8. FT-IR spectra of Fe_3O_4NPs (A_1), GO (A_2), 3D-GO/PVA (A_3), 3D-GO/PVA/Fe_3O_4 (A_4), PVA (A_5), and (3D-GO/PVA/Fe_3O_4)-PPL composites (B_6) and PPL (B_7).

3.2. Immobilization of enzyme

3.2.1. Effects of temperature, enzyme concentration, adsorption time, and pH on enzyme activity

The effect of temperature on enzyme activity was firstly studied. The result is shown in Fig. 9A. With increasing the temperature from 25 to 60 °C, the enzyme activity was changed, the optimum temperature was 40 °C for immobilized enzyme, and was 35 °C for free enzyme. As shown in Fig. 9A, the immobilized enzyme exhibited excellent activity compared with free enzyme when the temperature increased (at 60 °C), 64% of initial enzyme activity was remained for immobilized enzyme, while only 26% remained for free enzyme. The success at high temperatures were due to the strength of the enzyme-matrix interaction or the low limit of diffusion of the substrate [47]. This suggests that the interaction between the enzyme and the composites prevented the enzymes from the thermal denaturation to enhance the thermal stability of the enzyme [84]. The layered structure of nanofibers makes the enzyme more resistant to high temperature. Wang et al. [85] reported that lipase-immobilized polysulfone nanofibers retained 50% of their activity after being held at 50 °C for 100 min, while losing their activity in the free state. However, because the physical adsorption between the enzyme and the 3D-GO/PVA/Fe_3O_4 composites was weaker [86], the variation on activity of the enzyme was bigger at higher temperatures (35–60 °C). In addition, it was found that the maximum activity of enzyme was increased in the immobilized enzyme compared to the one in free enzyme, this suggests that the composites played an important role in enhancing the activity of the enzyme.

The effect of the enzyme concentration was also tested (Fig. 9B). The optimal concentration of the enzyme was 3.5 mg/mL for immobilized enzyme, and was 3.0 mg/mL for free enzyme. When high concentration of enzyme was applied to immobilization, an interaction between the enzyme and the enzyme could result in a conformational change and thereby reduced enzyme activity. On the other hand, the higher concentration of the enzyme may cause diffusion barrier or space barrier, which could hinder the effective

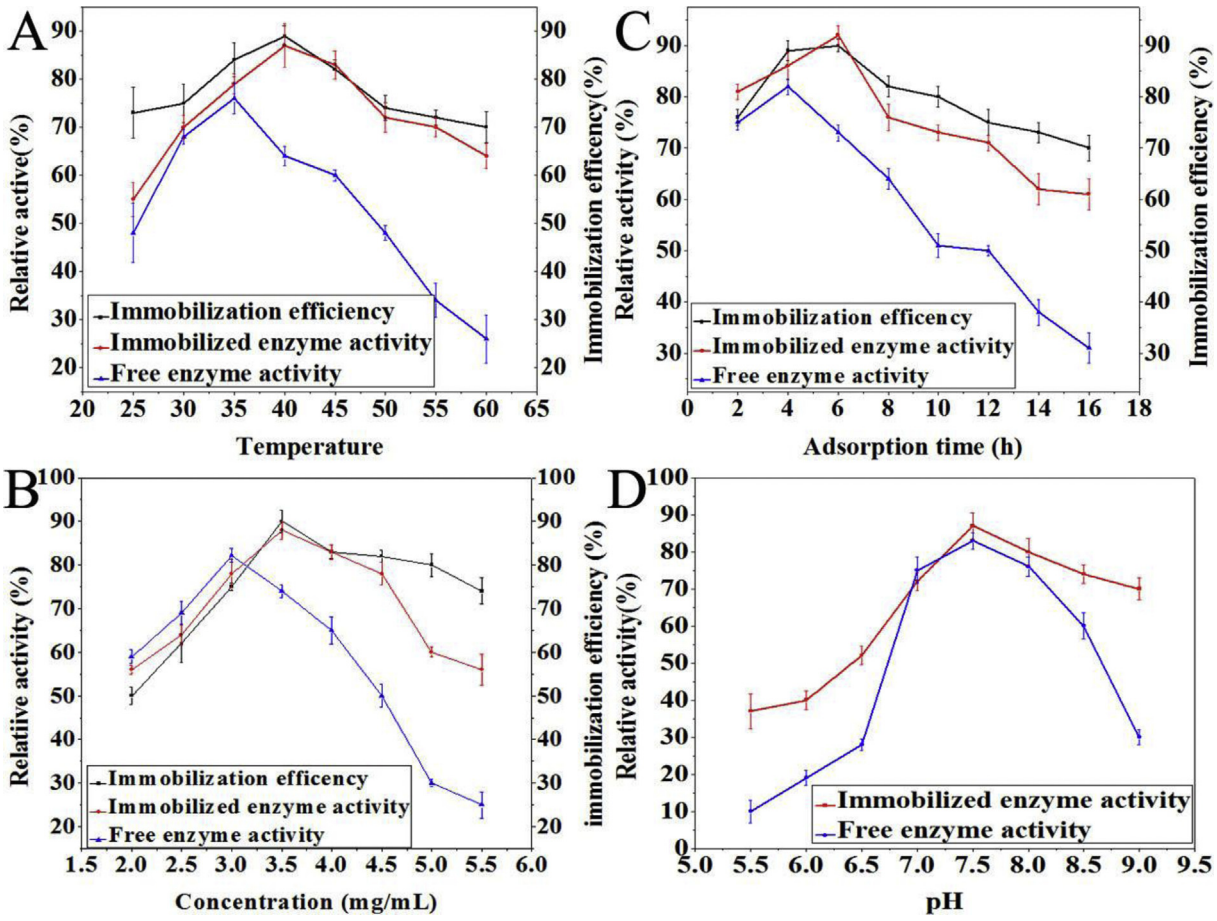

Fig. 9. Effects of temperature, concentration, and adsorption time, pH on immobilization efficiency and enzyme activity (Each data point was tested three times and the means and standard deviations were calculated by Excel).

contact between the enzyme and the substrate and also reduce the activity of the enzyme [87,88]. Additionally, the enzyme activity was also lowered at higher concentrations because the multilayer absorption might occur on the surface of composites and decreased more enzyme active sites [89,90]. Therefore, it is better to have a bigger specific surface area for the composites because it might provide a bigger space for enzyme reaction.

The effect of adsorption time on enzyme activity was investigated from 2 to 16 h (Fig. 9C). The optimum adsorption time was 6 h, and the immobilized enzyme activity was 91% which was much higher compared with other time. This indicated that the denaturation of the enzyme almost did not occur. However, with increasing the time (for example, over 6 h), the enzyme activity was significantly decreased due to the denaturation of the enzyme, multilayer adsorption of enzymes and aggregation of enzymes. Free enzymes placed in buffer solution for too long also easily led to the degeneration and deactivation, so that the free enzyme activity was decreased.

The effect of pH on enzyme activity was studied. The result is shown in Fig. 9D pH is one of the important parameters to affect the enzyme activity [91]. The optimum pH of the immobilized and free enzymes was 7.5. After the immobilization, (3D-GO/PVA/Fe_3O_4)-PPL showed a better stability in a wider pH range, especially in alkaline conditions (pH 7.5–9.0), which might be ascribed to the microenvironment due to the weak acidity of the composites [47,92]. The pH of the immobilized enzyme was more stable than that of free enzyme probably because the porous structure of the composites promoted the stability of enzyme or improved tolerance of enzyme to a higher pH condition [84,93]. These results indicate that the microenvironment around the immobilized enzyme can influence the enzyme activity cooperatively [94,95].

3.2.2. *Immobilized efficiency of the enzyme*

The effects of temperature (Fig. 9A, black line), enzyme concentration (Fig. 9B, black line), and adsorption time (Fig. 9C, black line) on immobilized efficiency of enzyme were explored by UV spectrophotometer for the 3D-GO/PVA/Fe_3O_4 composites. The results showed that the optimal values for the temperature, enzyme concentration, and adsorption time were 40 °C, 3.5 mg/mL, and 6 h in the process of enzyme immobilization. Under the optimal conditions, the best immobilized efficiency for (3D-GO/PVA/Fe_3O_4)-PPL was 91%, which was much higher than that for (GO/Fe_3O_4)-PPL (76%) [12]. As shown in Fig. 9A, B and C, the immobilized efficiency of the enzyme was firstly increased and then declined. When the enzyme concentration increased (over 3.5 mg/mL), enzyme was easily aggregated and multilayer absorption. The binds between enzyme and the composites were weaker by physical adsorption, which may cause the enzyme to fall off from the surface of composites, thereby reducing the immobilized efficiency. With increasing the temperature (over 40 °C), the enzyme will undergo the thermal denaturation and leads to the inactivation of the enzyme, therefore, the immobilized efficiency of the enzymes and composites is decreased. The increased adsorption time (over 6 h) may cause the denaturation of enzyme. In addition, with prolonging the time, the enzymes on the composites occurred multilayer absorption. Therefore, the immobilized efficiency of enzyme was

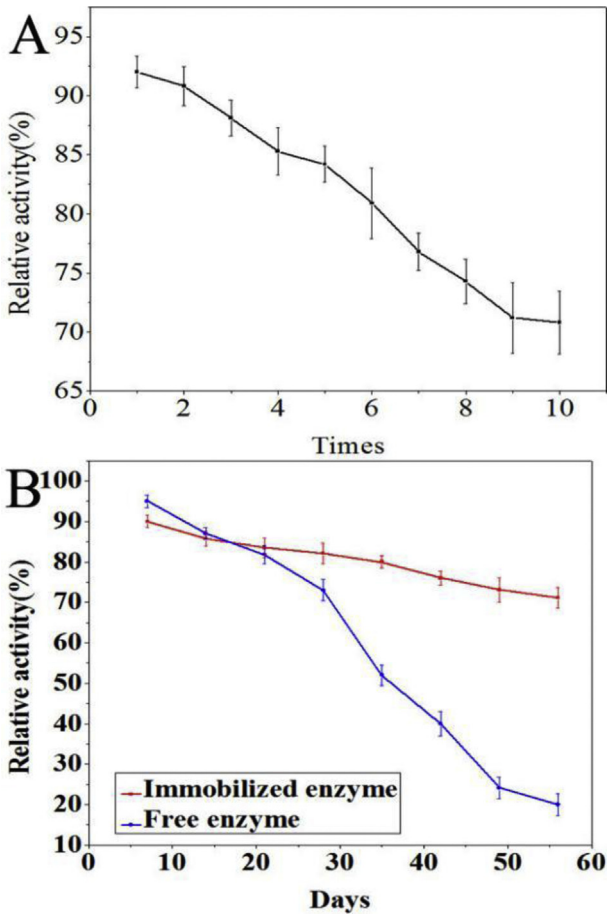

Fig. 10. Reusability and storage stability of enzyme activity (Each data point was tested three times and the means and standard deviations were calculated by Excel).

reduced with increasing the adsorption time.

3.2.3. Reusability and storage stability of the immobilized enzyme

Under optimal conditions, the reusability of the immobilized enzyme was probed for 6 times. The results are shown in Fig. 10A. After reusing for 6 times, the activity of the immobilized enzyme still remained about 70.8% of the initial activity (Fig. 10A). However, the interaction between enzyme and the composites is physical adsorption, which may cause the enzyme to fall off from the composites, so that the total enzyme activity is reduced and the variation on the enzyme activity is bigger.

The storage stability of the immobilized and free enzyme was tested every 7 days for total 56 days. The results are shown in Fig. 10B. The storage stability for free enzyme was very poor compared to the one for the immobilized enzyme. After 56 days, the immobilized enzyme still remained 71.1% of the initial activity, but the free enzyme only remained 20% of the initial activity. It indicated that the composites had a better rigid structure, which could improve the storage stability of the immobilized enzyme [12]. It indicated that the novel composites also played a key role for the reusability and storage stability. The composites have a stabilizing effect and the immobilized enzymes have a longer shelf life than free enzymes.

4. Conclusion

A 3D GO/PVA/Fe_3O_4 composite was prepared and characterized. The results indicate that it has a larger specific surface area, larger pore size. The 3D-GO/PVA/Fe_3O_4 composites have good magnetic properties that can be used for recycling by simply using an external magnet. Additionally, the three-dimensional porous structure can effectively improve the immobilization efficiency and enzyme activity. In terms of enzymology properties such as relative activity, reusability and storage stability, these composites exhibit great promise for industry applications.

Acknowledgments

The authors are grateful for the Project supported by the National Natural Science Foundation of China (Grant No.: 51473046) and Graduate innovation research projects for Qiqihar University (Item No.: YJSCX2016-018X).

References

[1] D.R. Dreyer, S. Park, C.W. Bielawski, R.S. Ruoff, Chem. Soc. Rev. 39 (2010) 228–240.
[2] K. Erickson, R. Erni, Z. Lee, N. Alem, W. Gannett, A. Zettl, Adv. Mater. 22 (40) (2010) 4467–4472.
[3] D. An, L. Yang, T.J. Wang, B.Y. Liu, Ind. Eng. Chem. Res. 55 (17) (2016) 4803–4810.
[4] Z.C. Wang, R.B. Wei, X.B. Liu, J. Mater. Sci. 51 (9) (2016) 4682–4690.
[5] M. Daly, C.H. Cao, H. Sun, Y. Sun, T. Filleter, C.V. Singh, ACS Nano 10 (2) (2016) 1939–1947.
[6] V. Georgakilas, J.N. Tiwari, K.C. Kemp, J.A. Perman, A.B. Bourlinos, K.S. Kim, R. Zboril, Chem. Rev. 116 (9) (2016) 5464–5519.
[7] S. Shamaila, A.K.L. Sajjad, A. Iqbal, Chem. Eng. J. 294 (2016) 458–477.
[8] Z.C. Wang, R.B. Wei, X.B. Liu, J. Electron. Mater. 46 (1) (2017) 488–496.
[9] S. Park, Y.Y. Shao, H.Y. Wan, P.C. Rieke, V.V. Viswanathan, S.A. Towne, L.V. Saraf, J. Liu, Y.H. Lin, Y. Wang, Electr. Commun. 13 (3) (2011) 258–261.
[10] D.S. Yu, L.M. Dai, J. Phys. Chem. Lett. 1 (2) (2009) 467–470.
[11] X.Y. Li, X.L. Huang, D.P. Liu, X. Wang, S.Y. Song, L. Zhou, H.J. Zhang, J. Phys. Chem. C 115 (44) (2011) 21567–21573.
[12] Y.B. Shao, T. Jing, J.Z. Tian, Y.J. Zheng, RSC Adv. 5 (126) (2015) 103943–103955.
[13] J.S. Luo, J.L. Liu, Z.Y. Zeng, C.F. Ng, L.J. Ma, H. Zhang, J.Y. Lin, Z.X. Shen, H.J. Fan, Nano Lett 13 (12) (2013) 6136–6143.
[14] L.T. Yan, H.Z. Wang, D. Huang, H.M. Luo, Eng. Sci. 1 (2018) 4–20 http://www.espublisher.com/doi/10.30919/es.180318.
[15] H.W. Wang, Z.J. Xu, H. Yi, H.G. Wei, Z.H. Guo, X.F. Wang, Nanomater. Energy 7 (2014) 86–96.
[16] X.Z. Wang, X.F. Zeng, D.P. Cao, Eng. Sci. 1 (2018) 55–63. http://www.espublisher.com/doi/10.30919/es.180325.
[17] H. Bi, F.Q. Huang, J. Liang, Y.F. Tang, X.J. Lü, X.M. Xie, M.H. Jiang, J. Mater. Chem. 21 (43) (2011) 17366–17370.
[18] Q. Luo, H. Ma, Q.Z. Hou, Y.X. Li, J. Ren, X.Z. Dai, Z.B. Yao, Y. Zhou, L.C. Xiang, H.Y. Du, Adv. Funct. Mater. 28 (2018), 1706777.
[19] T. Liu, K. Yu, L. Gao, H. Chen, N. Wang, L.H. Hao, T.X. Li, H.C. He, Z.H. Guo, J. Mater. Chem. A 5 (34) (2017) 17848–17855.
[20] H.Y. Du, C.X.X. Zhao, J. Lin, J. Guo, B. Wang, Z. Hu, Q. Shao, D. Pan, E.K. Wujcik, Z.H. Guo, Chem. Rec. (2018), https://doi.org/10.1002/tcr.201800008 (in press).
[21] T. Maiyalagan, X. Dong, P. Chen, X. Wang, J. Mater. Chem. C 22 (12) (2012) 5286–5290.
[22] W. Yu, C.Q. Liu, L. Qiu, P. Zhang, W.G. Ma, Y.N. Yue, H.Q. Xie, L.S. Larkin, Eng. Sci. 2 (2018) 1–3. http://www.espublisher.com/doi/10.30919/es8d710.
[23] X.F. Zhang, K.K. Yeung, Z.L. Gao, J.K. Li, H.Y. Sun, H.S. Xu, K. Zhang, M. Zhang, Z.B. Chen, M.M. Yuen, Carbon 66 (2014) 201–209.
[24] Y.Q. Guo, G.J. Xu, X.T. Yang, K.P. Ruan, T.B. Ma, Q.Y. Zhang, J.W. Gu, Y.L. Wu, H. Liu, Z.H. Guo, J. Mater. Chem. C 6 (12) (2018) 3004–3015.
[25] F. Yavari, Z.P. Chen, A.V. Thomas, W. Ren, H.M. Cheng, N. Koratkar, Sci. Rep. 1 (2011) 166.
[26] C.C. Kung, P.Y. Lin, F.J. Buse, Y. Xue, X. Yu, L. Dai, C.C. Liu, Biosens. Bioelectron. 52 (2014) 1–7.
[27] H. Liu, W.J. Huang, X.R. Yang, K. Dai, G.Q. Zheng, C.T. Liu, C.Y. Shen, X.R. Yan, J. Guo, Z.H. Guo, J. Mater. Chem. C 4 (20) (2016) 4459–4469.
[28] C. Hu, Z.Y. Li, Y.L. Wang, J.C. Gao, K. Dai, G.Q. Zheng, C.T. Liu, C.Y. Shen, H.X. Song, Z.H. Guo, J. Mater. Chem. C 5 (9) (2017) 2318–2328.
[29] H. Liu, M.Y. Dong, W.J. Huang, J.C. Gao, K. Dai, J. Guo, G.Q. Zheng, C.T. Liu, C.Y. Shen, Z.H. Guo, J. Mater. Chem. C 5 (1) (2017) 73–83.
[30] H. Liu, Y.L. Li, K. Dai, G.Q. Zheng, C.T. Liu, C.Y. Shen, X.R. Yan, J. Guo, Z.H. Guo, J. Mater. Chem. C 4 (1) (2016) 157–166.
[31] K.D. Gong, Q. Hu, Y.Y. Xiao, X. Cheng, H. Liu, N. Wang, B. Qiu, Z.H. Guo, J. Mater. Chem. A 6 (2018) 1119–11128, https://doi.org/10.1039/C8TA03066A.
[32] J.N. Huang, Y.H. Li, Y.H. Cao, F. Peng, Y.G. Cao, Q. Shao, H. Liu, Z.H. Guo, J. Mater. Chem. A (2018), https://doi.org/10.1039/C8TA02861C (in press).
[33] T.H. Yu, C.W. Liang, C.D. Kim, E.S. Song, B. Yu, IEEE Electron. Device Lett. 32 (8) (2011) 1110–1112.
[34] B.-J. Kim, G. Yang, M. Joo Park, J. Seop Kwak, K. Hyeon Baik, D. Kim, J. Kim,

Appl. Phys. Lett. 102 (16) (2013), 161902.
[35] Z.C. Wang, R.B. Wei, X.B. Liu, ACS Appl. Mater. Interfaces 9 (27) (2017) 22408–22419.
[36] Z.C. Wang, R.B. Wei, X.B. Liu, RSC Adv. 5 (107) (2015) 88306–88310.
[37] Z.C. Wang, R.B. Wei, X.B. Liu, J. Mater. Sci. Mater. Electron. 28 (10) (2017) 7437–7448.
[38] H.C. Gao, Y.M. Sun, J.J. Zhou, R. Xu, H.W. Duan, ACS Appl. Mater. Interfaces 5 (2) (2013) 425–432.
[39] Z.Y. Sui, Y. Cui, J.H. Zhu, B.H. Han, ACS Appl. Mater. Interfaces 5 (18) (2013) 9172–9179.
[40] Y. Tao, D.B. Kong, C. Zhang, W. Lv, M.X. Wang, B.H. Li, Z.H. Huang, F.Y. Kang, Q.H. Yang, Carbon 69 (2014) 169–177.
[41] R. Li, C.B. Chen, J. Li, L.M. Xu, G.Y. Xiao, D.Y. Yan, J. Mater. Chem. A 2 (9) (2014) 3057–3064.
[42] L.Y. Zhang, T. Wang, H.Y. Wang, Y. Meng, W.T. Yu, L.Y. Chai, Chem. Commun. (J. Chem. Soc. Sect. D) 49 (85) (2013) 9974–9976.
[43] X. Wang, X. Liu, H. Yuan, H. Liu, C. Liu, T. Li, C. Yan, X. Yan, C. Shen, Z. Guo, Mater. Des. 139 (2018) 372–379.
[44] C. Hu, Z. Li, Y. Wang, J. Gao, K. Dai, G. Zheng, C. Liu, C. Shen, H. Song, Z. Guo, J. Mater. Chem. C 5 (2017) 2318–2328.
[45] S. Nardecchia, D. Carriazo, M.L. Ferrer, M.C. Gutiérrez, F. del Monte, Chem. Soc. Rev. 42 (2) (2013) 794–830.
[46] H. Bai, C. Li, X.L. Wang, G.Q. Shi, Chem. Commun. (J. Chem. Soc. Sect. D) 46 (14) (2010) 2376–2378.
[47] Y.İ. Doğaç, İ. Deveci, B. Mercimek, M. Teke, Int. J. Biol. Macromol. 96 (2017) 302–311.
[48] S. Ghasemi, M. Heidary, M.A. Faramarzi, Z. Habibi, J. Mol. Catal. B Enzym. 100 (2014) 121–128.
[49] Y.B. Shao, T. Jing, J.Z. Tian, Y.J. Zheng, M.H. Shang, Chem. Pap. 69 (10) (2015) 1298–1311.
[50] C. Cheng, S. Li, S.Q. Nie, W.F. Zhao, H. Yang, S.D. Sun, C.S. Zhao, Biomacromolecules 13 (12) (2012) 4236–4246.
[51] J. Deng, B. Lei, A. He, X. Zhang, L. Ma, S. Li, C.S. Zhao, J. Hazard Mater. 263 (2013) 467–478.
[52] Y. Guo, G. Xu, X. Yang, K. Ruan, T. Ma, Q. Zhang, J. Gu, Y. Wu, H. Liu, Z. Guo, J. Mater. Chem. C 6 (2018) 3004–3015.
[53] T.Y. Wu, K.T. Lu, C.H. Peng, Y.S. Hong, C.C. Hwang, Mater. Res. Bull. 70 (2015) 486–493.
[54] M.M. Bradford, Anal. Biochem. 72 (1–2) (1976) 248–254.
[55] D.T. Tran, C.L. Chen, J.S. Chang, Appl. Energy 168 (2016) 340–350.
[56] S.F. Kiew, L.V. Kiew, H.B. Lee, T. Imae, L.Y. Chung, J. Contr. Release 226 (2016) 217–228.
[57] H. Yue, W. Wei, Z.G. Yue, B. Wang, N.N. Luo, Y.J. Gao, D. Ma, G.H. Ma, Z.G. Su, Biomaterials 33 (16) (2012) 4013–4021.
[58] C. Wang, M. Zhao, J. Li, J. Yu, S. Sun, S. Ge, X. Guo, F. Xie, B. Jiang, E. Wujcik, Y. Huang, N. Wang, Z. Guo, Polymer 131 (2017) 263–271.
[59] J.J. Liang, Y.F. Xu, D. Sui, L. Zhang, Y. Huang, Y.F. Ma, F.F. Li, Y.S. Chen, J. Phys. Chem. C 114 (41) (2010) 17465–17471.
[60] J. Lu, C.H. Deng, X.M. Zhang, P.Y. Yang, ACS Appl. Mater. Interfaces 5 (15) (2013) 7330–7334.
[61] L. Li, Y. Yang, J. Ding, J.M. Xue, Chem. Mater. 22 (10) (2010) 3183–3191.
[62] X.L. Peng, F. Xu, W.Z. Zhang, J.Y. Wang, C. Zeng, M.J. Niu, E. Chmielewská, Coll. Surf. A Phys. Eng. Asp 443 (2014) 27–36.
[63] J. Li, S.W. Zhang, C.L. Chen, G.X. Zhao, X. Yang, J.X. Li, X.K. Wang, ACS Appl. Mater. Interfaces 4 (9) (2012) 4991–5000.
[64] J.Y. Cao, Y.M. Wang, J.C. Chen, X.H. Li, F.C. Walsh, J.H. Ouyang, D.C. Jia, Y. Zhou, J. Mater. Chem. A 3 (27) (2015) 14445–14457.
[65] J. Lu, X. Jiao, D. Chen, W. Li, J. Phys. Chem. C 113 (10) (2009) 4012–4017.
[66] L.Z. Bai, D.L. Zhao, Y. Xu, J.M. Zhang, Y.L. Gao, L.Y. Zhao, J.T. Tang, Mater. Lett 68 (2012) 399–401.
[67] A.K. Mishra, S. Ramaprabhu, Desalination 282 (2011) 39–45.
[68] J.K. Han, Y.T. Shen, W. Feng, Nanoscale 8 (29) (2016) 14139–14145.
[69] Y.L. He, J.H. Li, L.F. Li, J.Y. Li, Mater. Lett 177 (2016) 76–79.
[70] H.Y. Zhu, Y.Q. Fu, R. Jiang, J. Yao, L. Xiao, G.M. Zeng, Bio Technol. 105 (2012) 24–30.
[71] H.F. Su, T. Wang, S.Y. Zhang, J.M. Song, C.J. Mao, H.L. Niu, B.K. Jin, J.Y. Wu, Y.P. Tian, Solid State Sci. 14 (6) (2012) 677–681.
[72] A. Lerf, H. He, M. Forster, J. Klinowski, J. Phys. Chem. B 102 (23) (1998) 4477–4482.
[73] X.Y. Liu, Y.F. Zhou, W.Y. Nie, L.Y. Song, P.P. Chen, J. Mater. Sci. 50 (18) (2015) 6113–6123.
[74] M.H. Wang, L.F. Cai, Q.X. Jin, H.Z. Zhang, S.M. Fang, X.W. Qu, Z.H. Zhang, Q.X. Zhang, Separ. Purif. Technol. 172 (2017) 217–226.
[75] B. Liang, W. Zhan, G.G. Qi, S.S. Lin, Q. Nan, Y.X. Liu, B. Cao, K. Pan, J. Mater. Chem. A 3 (9) (2015) 5140–5147.
[76] S.J. Xia, M.Z. Ni, T.R. Zhu, Y. Zhao, N.N. Li, Desalination 371 (2015) 78–87.
[77] Y.P. Tang, D.R. Paul, T.S. Chung, J. Membr. Sci. 458 (2014) 199–208.
[78] H. Liu, M. Dong, W. Huang, J. Gao, K. Dai, J. Guo, G. Zheng, C. Liu, C. Shen, Z. Guo, J. Mater. Chem. C 5 (2017) 73–83.
[79] N. Wang, P.R. Chang, P.W. Zheng, X.F. Ma, Appl. Surf. Sci. 314 (2014) 815–821.
[80] Y.L. Fan, G.Y. Wu, F. Su, K. Li, L. Xu, X.T. Han, Y.J. Yan, Fuel 178 (2016) 172–178.
[81] J.L. Pang, G.W. Zhou, R.R. Liu, T.D. Li, Mater. Sci. Eng. C 59 (2016) 35–42.
[82] M. Roberge, R.N. Lewis, F. Shareck, R. Morosoli, D. Kluepfel, C. Dupont, R.N. McElhaney, Prot Stru. Fun. Bio 50 (2) (2003) 341–354.
[83] X.N. Yang, X.B. Huang, R.Q. Hang, X.Y. Zhang, L. Qin, B. Tang, J. Mater. Sci. 51 (13) (2016) 6428–6435.
[84] C.F. Wang, G.W. Zhou, Y.Q. Xu, J. Chen, J. Phys. Chem. C 115 (45) (2011) 22191–22199.
[85] Z.G. Wang, J.Q. Wang, Z.K. Xu, J. Mol. Catal. B Enzym. 42 (1–2) (2006) 45–51.
[86] Y. Liu, J.Y. Chen, J. Bioact. Compat Polym. 31 (6) (2016) 553–567.
[87] J. Silva, G. Macedo, D. Rodrigues, R. Giordano, L. Gonçalves, Biochem. Eng. J. 60 (2012) 16–24.
[88] J.M. Palomo, M. Fuentes, G. Fernández-Lorente, C. Mateo, J.M. Guisan, R. Fernández-Lafuente, Biomacromolecules 4 (1) (2003) 1–6.
[89] H. Ghamgui, N. Miled, M. Karra-chaâbouni, Y. Gargouri, Biochem. Eng. J. 37 (1) (2007) 34–41.
[90] X.H. Li, X.N. Peng, Q.R. Wang, H.H. Zuo, X.H. Meng, B.J. Liu, Food Contr. 78 (2017) 48–56.
[91] M.J.P. Brito, C.M. Veloso, R.C.F. Bonomo, R.d.C.I. Fontan, L.S. Santos, K.A. Monteiro, Fuel Process. Technol. 156 (2017) 421–428.
[92] Q. Zhao, C. Guo, Y. Lu, L. Liu, J. Liang, J. Chen, Ind. Eng. Chem. Res. 55 (20) (2016) 5795–5804.
[93] V. Linsha, K. Aboo Shuhailath, K.V. Mahesh, A.A.P. Mohamed, S. Ananthakumar, ACS Sustain. Chem. Eng. 4 (9) (2016) 4692–4703.
[94] A.V. Paula, A.B. Moreira, L.P. Braga, H.F.d. Castro, L.M. Bruno, Quim. Nova 31 (1) (2008) 35–40.
[95] V.H. Perez, G.S. da Silva, F.M. Gomes, H.F. de Castro, Biochem. Eng. J. 34 (1) (2007) 13–19.